



CHAPTER ONE

INTRODUCTION

1.1 BACKGROUND AND MOTIVATION

The rapid growth in the demand for high-speed data rates for both business and residential applications, bandwidth on demand with high spectrum efficiencies and more reconfigurable systems and adaptivity to support multiple standards and multiple frequency bands have accelerated research and development for "last mile" broadband access technologies. Furthermore with developing countries recognizing the need for such technologies acting as an enabler for improved quality of life and economic revival, the global needs and challenges for broadband wireless access both in fixed and mobile type environments are increasing.

Fixed broadband wireless access systems face the challenges of providing high data rates and high quality wireless access over fading channels at almost wire-line quality as they are often compared to cable modems and asynchronous DSL (xADSL), which operate over fixed wire-line channels. The use of multiple antennas at both the transmitter (TX) and receiver (RX) side of a wireless link is one of the most promising technological means to address the challenges described. This is known as multiple-input-multiple-output (MIMO) antennas and when used in combination with signal processing and coding, it is proving to be a good implementation choice.

The major impairment of a wireless system is fading caused by destructive addition of multi-paths in the propagation medium and interference from other users. The performance improvement gained from MIMO is achieved through array gain, diversity gain, interference



suppression and multiplexing gain. In array gain, multiple antennas can coherently combine signals to increase the signal-to-noise ratio and thus improve coverage. This coherent combination can be employed at both the TX and RX and to be exploited, one needs channel state information (CSI). Since accurate CSI is difficult to obtain at the TX, array gain is more likely to occur at the RX. Spatial diversity through multiple antennas can be used to combat fading and significantly improve link reliability.

Diversity provides the RX with several (ideally independent) replicas of the transmitted signal and is therefore a powerful means to combat fading and interference. Time diversity (due to doppler spread) and frequency diversity (due to delay spread) are the more common forms [1], but in recent years the use of spatial or antenna diversity has received prominence. Diversity gain can be obtained at both the TX and RX end. Space-time codes (that is coding across space {antennas} and across time) developed in [2] help to realize the transmit diversity gain without knowing the channel at the TX. The idea of separating signal transmissions in a temporal and spatial domain has been previously implemented in systems which use multiple antennas at the RX side and a single antenna at the TX side, referred to as single-input-multiple-output (SIMO) systems [1]. Such systems are known to provide spatial/receiver diversity and together with maximum ratio combining can provide higher capacities. As mentioned above, multi-path fading is seen as one of the major impairments in wireless systems. With the use of multiple antennas in the MIMO systems, the multi-path environment is exploited through spatial multiplexing to achieve enhanced capacities, increasing linearly with N , where N is the minimum number of antennas on the TX and RX side [3–5]. Since the separation of the data streams happens in the spatial domain through the many different propagation paths in the rich scattering environment, one is able to transmit several data streams simultaneously at the same time within the same frequency interval and without increasing the overall transmit power of the system. The deep fades can be eliminated and the signal levels are higher and fluctuates much lesser over time [6, 7].

Interference suppression in multiple antennas can be used to suppress co-channel interference, hence increasing cellular capacity. For a fixed line MIMO system [8], where the channel changes is negligible and have perfect channel state information at the TX, one can use advanced schemes with waterfilling [9], yielding optimal performance of the MIMO system. Where the CSI is imperfect [10], the TX would rely on the average spatial statistics from the



RX, which could result in sub-optimal channel capacity [11]. In the case where the channel may experience fast fading but the average channel statistics do not [12], transmission schemes like eigen-beam forming can be applied. Ivrlač has shown in [13] that it is possible to achieve almost the same capacity as in the case with perfect CSI when average channel information was used.

In the final analysis, achieving the best performance can finally be attributed to having the most reliable channel characteristics. Since the performance of the MIMO system is highly channel dependent, it is essential to accurately characterize the channel by understanding the complex spatial behavior of the wireless MIMO channel [14]. Although statistical analysis [15] and ray tracing [16] are useful for modelling, these tools often do not represent the true channel behavior. Hence this research work is exactly addressing the above-mentioned issues, but with particular reference to the fixed broadband wireless indoor MIMO environment.

1.2 AUTHOR'S CONTRIBUTIONS AND OUTPUTS

1.2.1 Research Contribution

The author's main research contribution can be summarized as follows:

- The author presents a new geometrical model for the indoor environment with separate transmit and receive antenna correlation expressions in a closed form. Using this, the effect of capacity in such a system based on the effects of scattering, antenna element spacing, angular orientation of antenna array and number of antenna elements deployed, is determined. Using the results here as a basis the usefulness of a measurement campaign is suggested.
- Then a unique low cost wideband MIMO channel measurement system, developed in the University of Pretoria (UP) wireless research laboratory, for the measurement campaign undertaken at 2.4 GHz and 5.2 GHz using uniform linear arrays (ULA) and uniform circular arrays (UCA), is presented.
- The different types of metrics which have been determined are presented so as to characterize the channel and describe the channel behavior. The concept of *frequency scaling* in MIMO systems has also been developed. Two new frequency scaling



models, one for capacity using a UCA and the other for spatial correlation for the ULA are contributed.

- Steinbauer's [17] work for the double directional radio channel is extended. New expressions for the double directional response is defined in terms of joint spatial power spectra for two different types of beamformer methods. The *frequency scaling* technique is then applied.
- A new method and the corresponding analysis are presented to determine the maximum entropy estimate of the full joint TX/RX MIMO channel covariance matrix, where knowledge of only the separate TX and RX covariance is assumed. This is then compared to the well known Kronecker model [18].

1.2.2 Journal Publications

The following peer reviewed and accredited journal articles have been published by the author as part of his research activities.

- B.T. Maharaj, J.W. Wallace, L.P. Linde and M.A. Jensen, "Frequency scaling of spatial correlation from co-located 2.4 GHz and 5.2 GHz wideband indoor MIMO channel measurements", *Electronics Letters*, vol. 41, no. 6, pp.336-338, March 2005.
- B.T. Maharaj, J.W. Wallace, L.P. Linde and M.A. Jensen, "Linear dependence of double directional spatial power spectra at 2.4 and 5.2 GHz from indoor MIMO channel measurements", *Electronics Letters*, vol. 41, no. 24, pp. 1138-1340, November 2005.
- B.T. Maharaj and L.P. Linde, "Geometric modelling of a spatially correlated MIMO fading channel", *SAIEE Africa Research Journal*, IEEE/SAIEE-AFRICON '04 Special Issue, vol. 97, no. 2, pp. 191-197, June 2006.
- B.T. Maharaj, J.W. Wallace, L.P. Linde and M.A. Jensen, "A low cost open-hardware wideband MIMO wireless channel sounder", *IEEE Transactions in Instrumentation and Measurement*, completed first review, July 2007.

1.2.3 Conference Proceedings

The author's research work as reflected in this thesis, contributed the following outputs through publications in the following peer reviewed and accredited conference proceedings:



- B.T. Maharaj and L.P. Linde, "Capacity for spatial-temporal correlated MIMO fading channel", *Proceedings of IEEE AFRICON 2004*, vol. 1, pp.269-274, Gaborone, Botswana, September 2004.
- B.T. Maharaj, J.W. Wallace, L.P. Linde and M.A. Jensen, "A cost-effective wideband MIMO channel sounder and initial co-located 2.4 GHz and 5.2 GHz measurements", in *Proc. 2005 IEEE International Conference on Acoustics, Speech and Signal Processing (ICASSP)*, vol. 3, Philadelphia, PA, USA, 18-23 March 2005, pp. 981-984.
- B.T. Maharaj, J.W. Wallace, L.P. Linde and M.A. Jensen, "Co-located indoor 2.4- and 5.2- GHz MIMO channel measurements: frequency scaling of capacity and correlation", in *Proceedings of 2005 IEEE International Conference on Telecommunications (ICT'05)*, Cape Town International Conference Centre, Cape Town, South Africa, May 2005, CD-ROM.
- B.T. Maharaj and L.P. Linde, "Frequency scaling of capacity for a co-located 2.4 GHz and 5.2 GHz wideband indoor MIMO circular array system", in *Proc. IEEE ICTe Africa*, KICC, Nairobi, Kenya, 17-21 May 2006, CD-ROM.
- B.T. Maharaj, J.W. Wallace and L.P. Linde, "MIMO channel modelling: the Kronecker model and maximum entropy", in *Proc.2007 IEEE Wireless Communications and Networking Conference (WCNC)*, Hong Kong, 18-23 March 2007, CD-ROM.

1.2.4 Invited Paper

- B.T. Maharaj, J.W. Wallace and M.A. Jensen, "Comparison of double-directional channel response at 2.4 and 5.2 GHz from indoor co-located wideband MIMO channel measurements", in *Proceedings of General Assembly of International Union of Radio Science (URSI-GA '06)*, URSI - GA'06, New Delhi, India, 23-29 October 2005.

1.2.5 Additional Contributions

These contributions were based on the work related to that done by the author either as work done through supervision or collaboration.

- B.T. Maharaj, J.W. Wallace and M.A. Jensen, "Experimental evaluation of the MIMO wideband channel temporal variation", in *Proceedings of General Assembly of*



International Union of Radio Science (URSI-GA '06), URSI - GA'06, New Delhi, India, 23-29 October 2005.

- B.B. Varghese and B.T. Maharaj, "A spatially correlated model for MIMO fading channels", in *Proceedings of 2005 IEEE International Conference on Telecommunication (ICT '05)*, Cape Town International Conference Centre, Cape Town, May 2005, CD-ROM.

1.3 OUTLINE OF THESIS

Chapter Two gives the reader an overview of the the description of the MIMO system and a brief introduction to MIMO channels. Some of the propagation based developments for geometric models, ray tracing, statistical modelling and measurements based are discussed. The double directional channel case is outlined and then the MIMO capacity for the case where no CSI information at the TX, is presented.

Having developed a geometric model, one needs to establish the accuracy of this model for a real indoor environment. Hence in Chapter Four the University of Pretoria's and Africa's first wideband 8 x 8 MIMO channel sounder is presented. The uniqueness of this system, compared to some of the commercial systems available, lies in the fact that it is largely constructed from off-the-shelf components, hence making it low cost and easily within reach of most research groups' budgets. A description of the system deployed for this research work is outlined and this is followed with the description of the indoor measurement environment where the measurement campaign was undertaken. Finally, an exposé of our data collection and calibration procedure is presented.

Having undertaken the measurement campaign, the data was analyzed and various metrics such as capacity, spatial correlation and joint TX/RX beamforming, which can be used to characterize the channel in Chapter Five, are looked at. Initially some bulk statistics are presented, and then capacity (eigenvalues) for this environment is evaluated at both 2.4 GHz and 5.2 GHz. The analysis for the indoor environment leads to the development of the *frequency scaling* model of capacity for the UCA. Modelling of the separate spatial correlation for the ULA is developed and the new model is analyzed, justifying its accuracy and also



establishing a new *frequency scaling* relationship. Finally, a joint TX/RX beamforming (eigenvectors) model is developed and a closed form expression is derived in order to determine the joint spatial power characteristics in the channel. This is then compared with the conventional Bartlett and the Capon Beamforming techniques both at 2.4 GHz and 5.2 GHz.

Chapter Six describes the mathematical development of a new approach using maximum entropy, where, in order to derive the full joint covariance, only on knowledge of the separate TX and RX covariances is required. This unique model is compared to one of the most popular and well known models, viz. the Kronecker model. This model has some improvement over the Kronecker model and also shows great potential for further research and investigation.

Based on the techniques, analysis and results presented, Chapter Seven summarizes the conclusions and offers opportunities for further research and investigations.



CHAPTER TWO

CHANNEL MODELLING: AN OVERVIEW

2.1 MIMO COMMUNICATION SYSTEM MODEL

A block diagram for a generalized MIMO wireless communication system can be represented as that shown in Figure 2.1, where the system is divided into the space-time coding and signal processing parts and then multiplexed onto the N_T transmitter elements and finally through the channel. It is assumed that a set of Q independent data streams represented by the symbol vector $\mathbf{b}^{(n)}$ is encoded into N_T discrete-time complex baseband streams $\mathbf{x}^{(n)}$ at the transmitter as described in [19], where n is the time index. These input symbols are then converted into discrete-time samples by coding in space across the N_T outputs and over time through sampling. This is then converted into a continuous-time baseband waveform, $\mathbf{X}(\omega)$, with ω being the frequency. This signal is then up-converted and fed into the N_T antennas after any filtering and amplification. At the receiver the signal is combined from the N_R channels to produce the continuous output vector waveform $\mathbf{Y}(\omega)$, which is then matched-filtered and sampled to produce the discrete-time baseband sample stream $\mathbf{y}^{(n)}$. This $\mathbf{y}^{(n)}$ signal is finally space-time decoded to generate the estimated transmitted symbols, $\hat{\mathbf{b}}^{(n)}$ for the Q independent data streams.

Hence the baseband MIMO input-output relationship can be expressed as

$$\mathbf{y}(t) = \mathbf{H}(t) * \mathbf{x}(t) + \mathbf{n}(t) \quad (2.1)$$

where $\mathbf{n}(t)$ is additive white Gaussian noise (AWGN) and $*$ denotes the convolution. $\mathbf{H}(t)$ is an $N \times M$ channel impulse response matrix. Equation (2.1) can also be written in the frequency

domain as

$$\mathbf{Y}(\omega) = \mathbf{H}(\omega)\mathbf{X}(\omega) + \mathbf{n}(\omega). \quad (2.2)$$

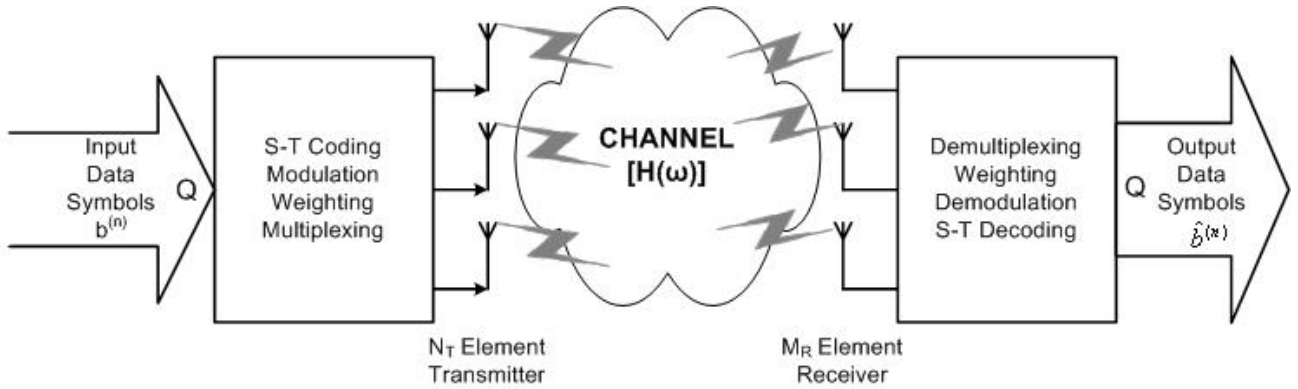


FIGURE 2.1: Block diagram of a generic MIMO wireless system

Each element $H_{ij}(\omega)$ represents the transfer function between the j^{th} transmit and i^{th} receive antenna. If the signal bandwidth is sufficiently narrow so that the channel response is constant over the system bandwidth (frequency flat channel), or when the wideband signals can be divided into narrowband frequency bins and processed independently, then equation (2.2) can be written as

$$\mathbf{y} = \mathbf{H}\mathbf{x} + \mathbf{n} \quad (2.3)$$

where \mathbf{H} is the narrowband MIMO channel matrix. In order to study the MIMO channel capacity, the elements of the narrowband MIMO channel matrix is assumed to be independent, identically distributed (iid) and at best, the data streams Q , would be equal to the rank of \mathbf{H} . However, in real MIMO systems factors such as antenna impedance matching, antenna element spacing, polarization properties and degree of scattering influence these and affect the system performance.



2.2 MIMO SYSTEM CAPACITY

In the single-input-single-output (SISO) system, the ergodic (mean) capacity of a random channel with $N_T = N_R = 1$ and an average transmit power constrained by P_T can be written as [20]

$$C = E_H \left\{ \max_{p(x): P \leq P_T} I(X; Y) \right\} \quad (2.4)$$

where P is the average power of a single channel codeword transmitted over the channel and E_H denotes the expectation over all channel realizations. The channel is thus defined [20] as the maximum of the mutual information between the input and the output over all statistical distributions on the input, that satisfy the power constraint. If each symbol at the transmitter is denoted by b , the average power constraint can be written as

$$P = E [|b|^2] \leq P_T. \quad (2.5)$$

Using (2.4), the ergodic (mean) capacity of a SISO system ($N_T = N_R = 1$) with a random complex channel gain h_{11} is given in ([15]) as

$$C = E_H \{ \log_2(1 + \rho \cdot |h_{11}|^2) \} \quad (2.6)$$

where ρ is the average signal-to-noise ratio (SNR) at the receiver branch. If $|h_{11}|$ is Rayleigh, $|h_{11}|^2$ follows the chi-squared distribution with two degrees of freedom [21]. Thus equation (2.6) can be written as [15]

$$C = E_H \{ \log_2(1 + \rho \cdot \chi_2^2) \} \quad (2.7)$$

where χ^2 is a chi-squared distribution random variable with two degrees of freedom.

Thus, using equation (2.7) one can show as in Figure 2.2 the Shannon capacity for a Gaussian channel and the capacity of a Rayleigh fading channel for a SISO channel, where the Rayleigh fading plot is as in [22].

For the MIMO system we can write the capacity of a random channel with power constraint P_T and transmit vector $\mathbf{X}(\omega)$, whose elements are complex Gaussian-distributed random variables, as

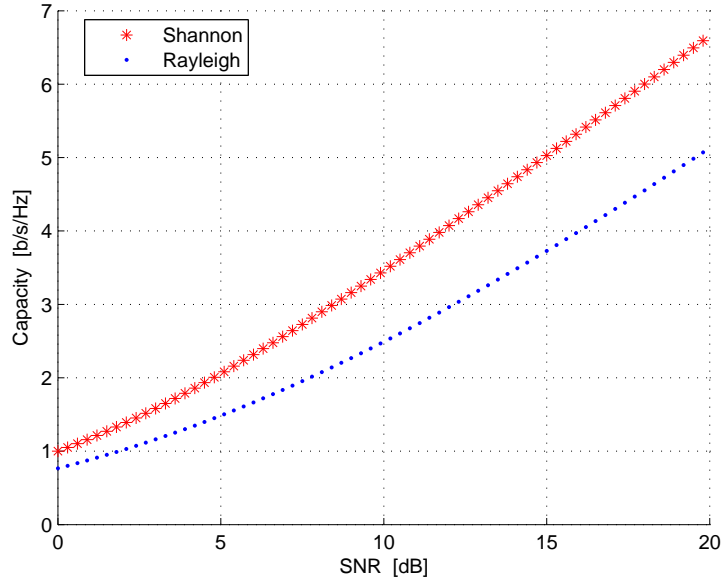


FIGURE 2.2: Ergodic capacity for a SISO channel vs SNR

$$C = E_H \left\{ \max_{p(\mathbf{x}): \text{tr}(\mathbf{R}_x) \leq P_T} I(\mathbf{x}, \mathbf{y}) \right\} \quad (2.8)$$

where $\mathbf{R}_x = E \{ \mathbf{x}\mathbf{x}^H \}$ is the diagonal elements of the transmit covariance representing the transmit power from each antenna, $\text{tr}(\cdot)$ denotes the trace, P_T is the total transmit power limited by the constraint $\text{tr}(\mathbf{R}) \leq P_T$ and $E\{\cdot\}$ is the expectation.

Now the ergodic (mean) capacity for a complex additive white Gaussian noise (AWGN) MIMO channel can be expressed as [9], [15]

$$C = E_H \left\{ \log_2 \left[\det \left(\mathbf{I}_{N_R} + \frac{P_T}{\sigma^2 N_T} \mathbf{H}\mathbf{H}^H \right) \right] \right\} \quad (2.9)$$

which can also be written as

$$C = E_H \left\{ \log_2 \left[\det \left(\mathbf{I}_{N_R} + \frac{\rho}{N_T} \mathbf{H}\mathbf{H}^H \right) \right] \right\} \quad (2.10)$$

where the average signal-to-noise ratio (SNR) is $\rho = \frac{P_T}{\sigma^2}$ at each of the receiver branch antenna elements.

The MIMO channel capacity can also be analyzed from equation (2.10) by using the eigenvector decomposition (EVD) [19] or singular value decomposition (SVD). Hence, the



product $\mathbf{H}\mathbf{H}^H = \xi\mathbf{\Lambda}\xi^H$, where ξ is the eigenvector matrix with orthonormal columns and $\mathbf{\Lambda}$ is a diagonal matrix with the eigenvalues on the main diagonal. Thus, equation (2.10) can be re-written as

$$C = E_H \left\{ \log_2 \left[\det \left(\mathbf{I}_{N_R} + \frac{\rho}{N_T} \xi \mathbf{\Lambda} \xi^H \right) \right] \right\} \quad (2.11)$$

If the SVD is used, then one can write

$$\mathbf{H} = \mathbf{U}\mathbf{S}\mathbf{V}^H \quad (2.12)$$

where \mathbf{U} and \mathbf{V} are unitary matrices and \mathbf{S} is a matrix with singular values on the main diagonal. The number of non-zero singular values, k , on the diagonal of \mathbf{S} gives the rank of the channel matrix, where the rank can be generally expressed as

$$\text{rank}(\mathbf{H}) = k \leq \min \{N_T, N_R\} \quad (2.13)$$

Now one can re-write (2.11) using (2.13) and noting that the determinant of a unitary matrix equals 1, one obtains

$$C = E_H \left\{ \sum_{i=1}^k \log_2 \left(1 + \frac{\rho}{N_T} \lambda_i \right) \right\} \quad (2.14)$$

where λ_i is the eigenvalues of the diagonal matrix $\mathbf{\Lambda}$. The ideal maximum capacity would be attained when each of the N_T transmitted signals is received by the same set of N_R receiver antennas without any interference.

With optimal combining at the RX and only receive diversity (ie. $N_T = 1$), one can write the channel capacity as

$$C = E_H \left\{ \log_2 \left(1 + \rho \cdot \chi_{2N_R}^2 \right) \right\} \quad (2.15)$$

where $\chi_{2N_R}^2$ is a chi-distributed random variable with $2N_R$ degrees of freedom. As in [15], for N_T transmit antennas and optimal combining between the N_R receive antennas, the capacity can be written as

$$C = E_H \left\{ N_T \log_2 \left[1 + \frac{\rho}{N_T} \chi_{2N_R}^2 \right] \right\}. \quad (2.16)$$

Figure 2.3 shows the implementation of equation (2.16), which represents the ergodic capacity upper bound of a Rayleigh fading MIMO channel with $N_T = N_R = 8$, when compared to a SISO channel with the Shannon capacity bound. Although this is a special case, it proves the inherent potential and research imperatives that need to be undertaken so as to exploit this opportunity of improved capacity in wireless communications, for example [2, 23–25].

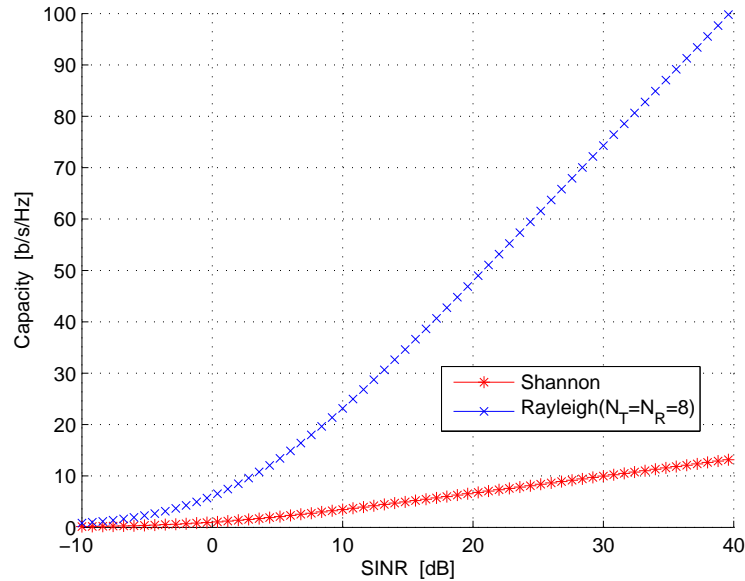


FIGURE 2.3: Comparison of Shannon capacity for SISO and ergodic capacity for Rayleigh fading MIMO Channels.

2.2.1 Water-Filling Capacity

The capacity can be obtained if one can determine the covariance \mathbf{R}_x that will maximize equation (2.8). Having been able to show \mathbf{H} in terms of the SVD as in (2.12), and since \mathbf{V} is unitary, one can write

$$\mathbf{x}' = \mathbf{V}^H \mathbf{x} \quad (2.17)$$

and

$$\mathbf{R}'_x = E \{ \mathbf{x}' \mathbf{x}'^H \} = \mathbf{V}^H \mathbf{R}_x \mathbf{V} \quad (2.18)$$

Using equation (2.18), it is shown in [26] that to maximize equation (2.8), \mathbf{R}'_x must be diagonal.

The capacity expression can then be written as [19]

$$C = \max_{\{R'_x: \sum_i R'_{x,ii} \leq P_T\}} \sum_{i=1}^{N_R} \log_2 \left(1 + \frac{S_{ii}^2 R'_{x,ii}}{\sigma^2} \right) \quad (2.19)$$

where $R'_{x,ii}$ represents the optimal transmit power on the i^{th} un-encoded stream and S_{ii}^2 is the power gain of the i^{th} eigenchannel. $R'_{x,ii}$ can be maximized in (2.19) by using Lagrange multipliers in order to obtain a waterfilling solution [20, 26–28]. The waterfilling method allocates power proportionally to the high-gain channels and generally would not use the weaker channels. As shown in [29], by using the waterfilling technique, one can have increased capacity by exploiting the improvement in the quality of the channels.

2.2.2 Uninformed Transmitter Capacity

When the transmitter does not have channel state information (that is it does not know \mathbf{H}), it would divide the power equally among all the N_T transmitter antennas. This implies that $\mathbf{R}_x = (P_T/N_T)\mathbf{I}$ and substituting this into (2.8) results in the uninformed transmitter capacity [15].

$$C_{UT} = \log_2 \left| \mathbf{I} + \frac{P_T}{N_T \sigma^2} \mathbf{H}\mathbf{H}^H \right| \quad (2.20)$$

2.2.3 Diversity and Spatial Multiplexing

In traditional antenna diversity the TX is used to send duplicate copies of the same information to the RX so as to increase the reliability of detection. With MIMO one would have the capability of exploiting the channel spatial degrees of freedom as it enables one to send distinctly different streams of information through the channel, hence increasing the throughput and spectral efficiency. Depending on the application and quality of service requirement, this combination of diversity and spatial multiplexing can vary as described in [30].

Diversity systems used for reducing branch signal correlation are also applicable to improving MIMO systems' performance. Low correlation is a good indicator for MIMO system performance [31], but need not necessarily be a sufficient condition. The pinhole or keyhole channel could exist as described in [32–35], where there is high correlation but also high capacity. This motivates a case for importance of knowledge of the channel and the



propagation environment having rich scattering.

Low correlation is achieved when each antenna provides a unique weighting to each multipath component based on its direction of departure (DOD) and direction of arrival (DOA). Systems would generally use a combination of the weighting based on the arrival phase due to antenna location (spatial diversity) or on magnitude and phase due to antenna pattern or polarization characteristics.

Generally low correlation would occur for a large set of multipaths with large angular spread created by a rich scattering environment. This could produce a low SNR, which in turn decreases the channel capacity [31, 36]. The effect that antenna spacing (branch correlation) has on capacity has been investigated in [14], where it is shown that a wide antenna spacing resulted in a low correlation for a 2×2 channel and as the antenna spacing decreased due to the adding of more elements across a constant array length, the capacity per antenna dropped due to the higher correlation between adjacent elements. Similar phenomena was also reported in [37–41], where it is shown that the increased signal correlation degrades the MIMO system performance.

2.3 MULTIPATH CHARACTERIZATION

2.3.1 Beamforming

Beamforming and subspace-based methods form part of the spectral-based approach [42]. One 'steers' the array in one direction at a time and measure the output power. The maximum power at each of the steering positions gives the direction of arrival (DOA) estimates. This output can be written as a linear combination given by

$$y(t) = \sum_{l=1}^L w_l^* x_l(t) = \mathbf{w}^H \mathbf{x}(t) \quad (2.21)$$

where \mathbf{x} is the array output vector (for example DOA emitter signals) and \mathbf{w} is the weighting vector.

For samples $y(1), y(2), \dots, y(N)$; the output power is measured by



$$P(\mathbf{w}) = \frac{1}{N} \sum_{l=1}^N |y(t)|^2 = \frac{1}{N} \sum_{l=1}^N \mathbf{w}^H \mathbf{x}(t) \mathbf{x}^H(t) \mathbf{w} = \mathbf{w}^H \hat{\mathbf{R}} \mathbf{w} \quad (2.22)$$

where $\hat{\mathbf{R}}$ is the sample covariance matrix and can be written as [42]

$$\hat{\mathbf{R}} = \frac{1}{N} \sum_{t=1}^N \mathbf{x}(t) \mathbf{x}^H(t) \quad (2.23)$$

2.3.2 Bartlett Beamformer

The Bartlett or conventional beamformer dates back to World War II and it is an extension of the Fourier-based spectral analysis to spatio-temporally sampled data [43]. For a particular array geometry (for example the UCA) this algorithm maximizes the power of the beamforming output for a given input signal.

If one wishes to maximize the output power from a certain direction θ , then the array output, corrupted with additive noise, can be written in terms of the steering vector, \mathbf{a} , and the baseband signal waveform, $s(t)$ as

$$\mathbf{x}(t) = \mathbf{a}(\theta) s(t) + \mathbf{n}(t) \quad (2.24)$$

The maximum output power can be formulated and the weighting vector can be determined [42, 43] as

$$\mathbf{w}_{BF} = \frac{\mathbf{a}(\theta)}{\sqrt{\mathbf{a}^H(\theta) \mathbf{a}(\theta)}} \quad (2.25)$$

This weight vector can be interpreted as a spatial filter, which has been matched to the impinging signal. One can then insert equation (2.25) into equation (2.22) to obtain the spatial power spectrum as [42]

$$P_{BF}(\theta) = \frac{\mathbf{a}^H(\theta) \hat{\mathbf{R}} \mathbf{a}(\theta)}{\mathbf{a}^H(\theta) \mathbf{a}(\theta)} \quad (2.26)$$

For the UCA case the steering vector $\mathbf{a}(\theta)$ can be written as

$$\mathbf{a}_{UCA} = \exp(j2\pi(x \cos \theta + y \sin \theta)) \quad (2.27)$$

where x and y are the resolved co-ordinates for each antenna element as shown in Figure 2.4, thus making it possible to determine the beamforming spectra versus DOA.

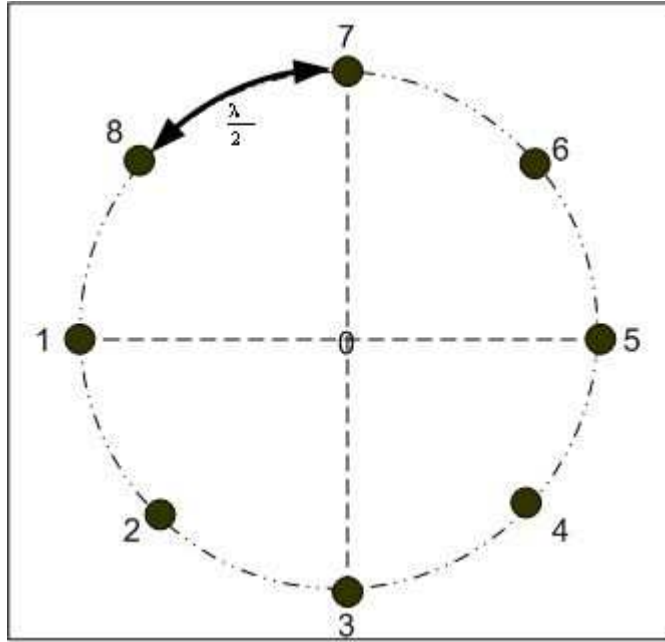


FIGURE 2.4: Uniform circular 8 element antenna array layout

2.3.3 Capon Beamformer

Capon's beamformer attempts to minimize the power contributed by noise and any signals coming from other directions other than θ , while still maintaining a fixed gain in the direction of θ . Capon [44] proposed a different method based on the optimization problem formulated as

$$\begin{aligned} \min_{\mathbf{w}} P(\mathbf{w}) & \quad (2.28) \\ \text{subject to } \mathbf{w}^H \mathbf{a}(\theta) &= 1 \end{aligned}$$

where $P(\mathbf{w})$ is as defined in equation (2.22). Using the technique of Lagrange multipliers, one can find the optimal \mathbf{w} as [44]

$$\mathbf{w}_{CAP} = \frac{\hat{\mathbf{R}}^{-1} \mathbf{a}(\theta)}{\mathbf{a}^H \hat{\mathbf{R}}^{-1} \mathbf{a}(\theta)} \quad (2.29)$$

and inserting equation (2.29) into equation (2.22) leads to the spatial spectrum

$$P_{CAP}(\theta) = \frac{1}{\mathbf{a}^H(\theta) \hat{\mathbf{R}}^{-1} \mathbf{a}(\theta)} \quad (2.30)$$



Consequently, using equations (2.30) and (2.27) one can determine the spatial power for DOA. The Capon beamformer generally performs better than the Bartlett beamformer as it uses every available degree of freedom to concentrate the received energy along one direction, since the constraint minimizes $\mathbf{P}(\mathbf{w})$ as compared to the Bartlett beamformer which maximizes the output power. However the Capon beamformer can suffer from noise enhancement as a result of \mathbf{R}^{-1} as shown in (2.30) and is also dependent on the SNR and array aperture in resolving the spectral power content.

2.3.4 Double-Directional Channel Model

The double directional concept includes angular information which is defined in terms of paired discrete plane-wave departures and arrivals at both the TX and RX. This is described through the propagation channel approach [45] where the TX and RX antennas can be excluded.

Generally, the local propagation scenario can be represented in a system-related fashion by the multi-dimensional spreading function (MDSF) as [46]

$$s = (\nu, \tau, \varphi_R, \varphi_T) \quad (2.31)$$

where ν is the Doppler shift, τ is the delay, φ_R is the angle of arrival at RX and φ_T is the angle of departure at the TX.

One can express the input-output relationship through convolution of the MDSF in multi-dimensions. The approach used here is to describe the directional case via the time-dependent complex channel impulse response (CIR), as $h(t, \tau, \varphi_R)$ and the non-directional case as $h(t, \tau)$. The RX antenna coherently sums up components from all directions, weights them with the complex antenna pattern $g_R(\varphi_R)$, and thus integrates over the respective angular domain as [46]

$$h(t, \tau, \varphi_R) = \int_{-\pi}^{\pi} h(t, \tau, \varphi_T, \varphi_R) g_T(\varphi_T) d\varphi_T \quad (2.32)$$

$$h(t, \tau) = \int_{-\pi}^{\pi} h(t, \tau, \varphi_R) g_R(\varphi_R) d\varphi_R \quad (2.33)$$

where T and R represent the transmit and receive, respectively.



From the above, one observes that $h(t, \tau)$ is the angle integrated directional channel impulse response $h(t, \tau, \varphi_R)$, while the directional channel impulse response is the angle integrated double directional channel impulse response $h(t, \tau, \varphi_R, \varphi_T)$. Hence, the propagation channel is now described by the double directional channel response.

The double directional channel model [45, 46] separates the radio transmission chain into the TX antenna, double directional channel and the RX antenna. The TX antenna would essentially distribute the RF energy into the respective directions of departure (DOD), while the RX antenna would collect and capture the signal from the different angles of arrival (AOA) by weighted combination. The double directional channel includes all resolvable propagation paths, L , between the TX and RX and can be expressed by the CIR as shown in [46].

Now the wideband MIMO channel response can be computed for any antenna constellation as [46]

$$h(t, \tau, x_R, x_T) = \sum_{i=1}^L h(t, \tau, \varphi_{R,i}, \varphi_{T,i}) g_R(\varphi_{R,i}) g_T(\varphi_{T,i}) e^{-j\vec{k}^T(\varphi_{R,i})\vec{x}_R} e^{-j\vec{k}^T(\varphi_{T,i})\vec{x}_T} \quad (2.34)$$

where L is the overall number of multipath components aggregated over all domains, \vec{x}_R and \vec{x}_T are the vectors of the chosen element position measured from an arbitrary but fixed reference point on the corresponding array. The exponential k -terms in (2.34) are defined as:

$$\vec{k}^T(\varphi) \cdot \vec{x} = \frac{2\pi}{\lambda} (x \cos \varepsilon \cos \varphi + y \cos \varepsilon \sin \varphi + z \sin \varepsilon) \quad (2.35)$$

When the true channel behavior is represented by the above equations, the multipath parameters may then be measured using conventional beamforming [42], basis matching techniques [47], or parametric estimation algorithms such as ESPRIT [42, 48, 49].

2.3.5 Ray Tracing

Ray tracing is a technique that allows multipath routes to be predicted from positions off walls and other reflecting surfaces through the creation of either two-dimensional (2D) or three-dimensional (3D) models from modelling the electromagnetic excitation in that



environment. This allows not only the signal strengths of the multipath components, but also their angles of arrival and departure from the transmitter and receiver to be estimated, hence allowing one to determine the channel capacity.

The ray tracing approach can be extremely computationally intensive [16], especially if one has to include line-of-sight (LOS), reflected, transmitted, diffracted, scattered and some combined rays. Therefore, generally simple scenarios are considered and have emerged as the most popular technique for the analysis on site-specific scenarios [50–52]. Some of the more commonly used ray tracing methods are the shooting and bouncing ray launching algorithm, the image method and the hybrid acceleration method of ray tracing algorithms [53].

Ray tracing techniques have shown some promise in predicting large scale path loss variation, with the average error standard deviation being 7.2 [53], but preliminary comparisons of ray tracing with MIMO measurements indicated that the simulations tended to underestimate the capacity [54]. However, recent propagation prediction and site planning for an indoor environment yielded an error standard deviation of less than 3dB [55] for a specific case. There have been some promising results for AOA and AOD when compared with measurements which, when combined with the random distribution of the phase [56, 57], can be used to characterize the channel. However, integration of the ray-tracing approach for outdoor/indoor propagation through windows and reflection as well as transmission through complex walls with 3D would be required to improve the accuracy of the technique [58, 59] and enable it to be more generally used.

Although some work using ray tracing to predict MIMO capacity variation with array location and antenna spacing [40, 60] and spatial power signature in the channel [61] have been reported, more opportunity exists for research into the modelling and computational efficiency versus accuracy in this complex arena.

2.3.6 Geometric Models

Geometric models capture the spatial multipath behavior range in complexity and can be represented by various physical properties [62]. For the narrowband case they can be the received signal power and time varying amplitude (fading) distribution, but for wideband



systems properties such as angle of arrival (AOA), angle of departure (AOD), time of arrival (TOA), time delay spread and adaptive array antenna geometries become relevant in order to improve the accuracy of the representation of the physical channel. Some of the models briefly mentioned hereafter will vary in the complexity of the geometry and the scattering mechanisms considered, largely due to computational and numerical limitations in finding closed form solutions.

In the one-ring model [37], the transmitter (TX) is assumed to be elevated and hence, assumed to be unobstructed by local scattering, while the receiver (RX) is surrounded by scatterers. There is also no-line-of-sight component between TX and RX, the scattering is uniformly distributed at the RX across some angle θ , so that each ray is assumed to be reflected only once and all rays reach the receive array with the same power. In [37], they derive an equation for the channel covariance which is in terms of some of the geometrical parameters and can be evaluated by numerical analysis. Similarly the two-ring model [63] is derived where there is a ring of scatterers at both the TX and RX.

In [64, 65] a model is proposed that uses the von Mises angular probability density function (PDF) as the angular PDF at only the RX and also considers the Doppler spread distribution. The von Mises angular PDF is proposed as a versatile model for the representation of the angular PDF as it compared well with measured data [66]. Furthermore it has a scattering parameter κ that can be varied depending on the scattering for that particular environment. In [64] the channel covariance can be written as

$$\begin{aligned}
 E [H_{p,n}(t)H_{q,m}^H(t + \tau)] &= \frac{\exp [jc_{pq} \cos(\alpha)]}{I_0(\kappa)} I_0(\{\kappa^2 - a^2 - b_{nm}^2 - c_{pq}^2 \gamma^2 \sin^2(\alpha) \\
 &\quad + 2ab_{nm} \cos(\beta - \phi) \\
 &\quad + 2c_{pq} \gamma \sin(\alpha)[a \sin(\phi) - b_{nm} \sin(\beta)] \\
 &\quad - j2\kappa[a \cos(\mu - \phi) - b_{nm} \cos(\mu - \beta) \\
 &\quad - c_{pq} \gamma \sin(\alpha) \sin(\mu)]\}^{1/2})
 \end{aligned} \tag{2.36}$$

and the von Mises PDF is defined by the angular PDF, $p(\theta)$ as

$$p(\theta) = \frac{\exp[\kappa \cos(\theta - \mu)]}{2\pi I_0(\kappa)} \tag{2.37}$$



where d_{pq} and d_{nm} are the element spacing at the BS and MS respectively, ϕ is the direction of the moving MS, τ is the relative time difference between the two links $H_{p,n}$ and $H_{q,m}$, $f_D = v/\lambda$ is the Doppler shift with v being the speed of the MS, $\theta \in [-\pi, \pi)$, μ is the mean AOA at the MS and $I_0(\cdot)$ is the zero order modified Bessel function.

The above model has a closed form expression and can therefore be used to analytically study the channel covariance and the impact of the various model parameters on the capacity, both for LOS and NLOS scenarios. This model is adapted for an indoor scenario where scattering at both the TX and RX is considered, and is analyzed in Chapter 3.

The distributed scattering model was proposed in [67] to describe outdoor MIMO propagation channels. Here the TX and RX are obstructed by the surrounding scatterers which are located at a distance large enough from the TX and RX so that one can assume the signals as plane waves. Assuming that there are a large number of scatterers (S), having random fading, the MIMO channel transfer function can be described by

$$\mathbf{H} = \frac{1}{\sqrt{S}} \mathbf{R}_{\theta_r, d_r}^{1/2} \mathbf{G}_r \mathbf{R}_{\theta_s, 2D_r/S}^{1/2} \mathbf{G}_t \mathbf{R}_{\theta_t, d_t}^{T/2} \quad (2.38)$$

where $\frac{1}{\sqrt{S}}$ is the normalization factor, \mathbf{G}_t and \mathbf{G}_r are random matrices with iid zero mean complex Gaussian elements, $\mathbf{R}_{\theta_t, d_t}$, $\mathbf{R}_{\theta_s, 2D_r/S}$, $\mathbf{R}_{\theta_r, d_r}$ are the correlation matrices seen from the transmitter, the virtual array and receiver respectively, d is the array element distance and θ_i is the AOA of the i^{th} scatterer.

In [68] a wideband SISO multipath channel model was proposed for the indoor scenario based on an indoor measurement campaign. The multipath components were observed to arrive in groups and therefore the scatterers could be separated into clusters. This Saleh-Valenzuela model was extended for MIMO channels in [69–71], taking into account the statistics of the AOA and AOD, giving the coefficient of the narrowband channel matrix as

$$H_{nm} = \int_{2\pi} \int_{2\pi} W_n^R(\theta^R) h(\theta^R, \theta^T) W_m^T(\theta^T) d\theta^T d\theta^R \quad (2.39)$$

where $W_q^P(\theta) = G_q^P \exp[j\psi_q^P(\theta)]$, with G_q^P being the antenna gain pattern, $\psi_q^P(\theta) = 2\pi[x_q^P \cos(\theta) + y_q^P \sin(\theta)]$, $P \in (T, R)$ and $q \in (m, n)$. This model was compared with narrowband indoor channel measurements and reported good accuracy in terms of channel capacity PDF.



A directional channel model developed by the European research initiative COST259 was reported in [72], and can be used to model different MIMO propagation channels. The double directional channel impulse response (DDCIR) was derived as

$$H_{nm}(t, \tau, \theta^R) = \int_{\theta^T} G_m^T(\theta^T) H_{nm}(t, \tau, \theta^R, \theta^T) d\theta^T \quad (2.40)$$

where $G_m^T(\theta^T)$ is the complex antenna pattern for the m^{th} transmit element, θ_R and θ_T are the corresponding AOA and AOD at the RX and TX respectively and m and n are the number of TX and RX elements respectively.

To simulate the channel as described in [72], a layered approach whereby different environments have been separated into three levels was followed. The top level is the cell type and each cell type includes the second level, namely the number of radio environments. For each of the radio environments, some propagation scenarios have been identified, hence forming the third level. Each of these levels have certain input parameters which are either known, measured or statistically obtained to model the channel.

Other known models are the Virtual Channel Model [73] and EM Scattering model as presented in [74–76], where the properties of the channel and antennas are taken into account. This model has two discs of scatterers for transmit and receive and the scatterers on each side are organized into clusters. The model includes antenna polarization properties through the antenna functions, consequently enabling one to also study depolarization.

Others [77–80] have also modelled the scatterers as discrete objects which can represent specific scatterers in the channel, or they can be defined by some statistical function such as a Poisson process in proximity of either the TX or RX. Assuming a single or double bounce scattering mechanism, the channel response can be determined. In real world channels it may not be possible to completely describe the channel by these limited number of parameters and one may be able to validate the geometric models that describe the radio channel in certain environments. Hence there will always be some limitation (which can be taken into account) to geometric modelling, but they will always form an important aspect to wireless channel characterization [81].



2.4 CONCLUSION

This chapter has presented an overview of some of the modelling techniques one could use to characterize a wireless channel, as well as some of the research activities that have been undertaken, and are still ongoing, aimed at reliably and accurately representing the electromagnetic propagation in the MIMO channel. The collective importance and integration of electromagnetic theory, signal processing and communication theory lends much opportunity for further research into MIMO channel modelling.